Seton Maria (Orcid ID: 0000-0001-8541-1367)
Muller R. Dietmar (Orcid ID: 0000-0002-3334-5764)
Zahirovic Sabin (Orcid ID: 0000-0002-6751-4976)
Williams Simon (Orcid ID: 0000-0003-4670-8883)
Cannon John (Orcid ID: 0000-0003-4749-5605)
Whittaker Jo (Orcid ID: 0000-0002-3170-3935)
Matthews Kara (Orcid ID: 0000-0003-3249-3869)
McGirr Rebecca (Orcid ID: 0000-0001-9439-8571)

A global dataset of present-day oceanic crustal age and seafloor spreading parameters

Maria Seton[1*], R. Dietmar Müller[1], Sabin Zahirovic[1], Simon Williams[1,2], Nicky M. Wright[3,4], John Cannon[1], Jo Whittaker[5], Kara J. Matthews[6], Rebecca McGirr[4]

[1]EarthByte Group, School of Geosciences, University of Sydney NSW 2006 Australia

[2]State Key Laboratory of Continental Dynamics, Department of Geology, Northwest University, Xi'an, China.

[3]Centre of Excellence for Climate Extremes, Australian National University, ACT 2601, Australia

[4]Research School of Earth Sciences, Australian National University, ACT 2601, Australia

[5]Institute for Marine and Antarctic Studies, University of Tasmania, TAS, 7001, Australia

[6]Arctic Institute of North America, University of Calgary, Canada

* Corresponding author: Maria Seton (maria.seton@sydney.edu.au)

Key Points:

- New oceanic crustal age grid and complementary grids of spreading rate, asymmetry, direction and obliquity are presented
- Mean oceanic crustal age of 64.2 million years is reported; slow and fast spreading systems are the most common by area
- All gridded datasets as well as the workflows are made freely available

This article has been accepted for publication and undergone full peer review but has not been through the copyediting, typesetting, pagination and proofreading process which may lead to differences between this version and the Version of Record. Please cite this article as doi: 10.1029/2020GC009214

Abstract

We present an updated oceanic crustal age grid and a set of complementary grids including spreading rate, asymmetry, direction and obliquity. Our dataset is based on a selected set of magnetic anomaly identifications and the plate tectonic model of Müller et al. (2019). We find the mean age of oceanic crust is 64.2 Myrs, slightly older than previous estimates, mainly due to the inclusion of pockets of Mesozoic aged crust in the Atlantic and Mediterranean and improvements to the Jurassic Pacific triangle. This older crust is partly compensated by additional Cenozoic-aged back-arc basin crust not included in previous models. The distribution of spreading modes based on area of preserved crust is relatively equal between slow (20–55 mm/yr) and fast (75–180 mm/yr) spreading systems at 33 and 39%, respectively. Crust transitional between fast and slow, or intermediate systems (55–75 mm/yr), cover 20% of the preserved ocean floor with much smaller proportions of crust formed at ultra-slow (5%) and super-fast (3%) spreading systems. Slow and intermediate spreading systems exhibit the most stable behavior in terms of spreading asymmetry and obliquity, with the widest distribution of obliquities occurring at ultra-slow spreading systems, consistent with present-day observations. Our confidence grid provides a complementary resource for non-experts to identify those parts of the age grid that are least well constrained. Our grids in 6, 2 and 1 arc-minute resolution as well as our python workflow, *isopolate*, used to compute our datasets are freely available in online repositories and on the GPlates data portal.

Plain Language Summary

The age of the ocean floor is one of the fundamental datasets for understanding plate tectonic processes. We have generated an updated present-day age grid of oceanic crust by incorporating recent improvements to the underlying plate motion model, magnetic anomaly identifications and fracture zones. The resultant mean age of the ocean floor is ~ 64 million years, slightly older than previous studies. We also present datasets showing various seafloor spreading parameters such as spreading rate, asymmetry, direction and obliquity. Slow and intermediate seafloor-spreading rates produce the most stable spreading behavior in terms of asymmtery and obliquity. Our datasets and workflows are freely available and can be used for multi-disciplinary scientific studies. Our maps are an effective visual tool to understand plate tectonic concepts and can be used for education and outreach.

1 Introduction

The world's oceans contain a variety of bathymetric features, such as abyssal hills, volcanic arcs and islands, fracture zones, mid-ocean ridge systems and volcanic plateaus, each with a distinctive composition, morphology and tectonic process by which they were created. While age constraints for many of these submarine features rely on direct sampling, the age of the abyssal plains flanking the mid-ocean ridge systems, which form the oceanic basement, can be inferred from remote sensing of the seafloor to generate a marine magnetic anomaly record. This allows for basin-wide mapping of the age of the oceanic crust and, together with an underlying plate motion model, can inform about seafloor-spreading processes, plate driving forces, mantle and ocean dynamics and form the basis of reconstructing the past configurations of the continents and oceans from the Mesozoic to present day.

The first digital global map of the present-day age of oceanic crust accompanied by an underlying global plate motion model was produced by Müller et al. (1997). This study provided an open-access netCDF grid at 6 arc minute resolution, a table of plate rotations and seafloor-spreading isochrons. Prior to this advance, maps were restricted to analogue or low resolution digital formats without the necessary information of how the age model was constrained, placing limits on their usefulness, accessibility and reproducibility. An update to Müller et al. (1997) was presented in Müller et al. (2008) and reflected new data and interpretations. Importantly, it filled many data gaps in the Mesozoic-aged crust in the Pacific and Indian oceans. Companion grids showing present-day seafloor-spreading rates, asymmetry, and age uncertainty were also computed. These previous generations of age and seafloor-spreading grids have been used to study a variety of earth processes including: global mantle flow (Coltice et al., 2013; Stadler et al., 2010); seafloor crustal thickness (Van Avendonk et al., 2017); crustal production (Seton et al., 2009); ocean chemistry (Müller et al., 2013); subduction dynamics (Becker et al., 2014); oceanic gravity and topography (Crosby & McKenzie, 2009; Steinberger, 2016); and ocean sedimentation (Dutkiewicz et al., 2017; Olson et al., 2016). More recently, regional age grid models have been developed (e.g. Gaina et al., 2017; Gaina et al., 2015; Pérez-Díaz & Eagles, 2017), which use alternative gridding algorithms, plate kinematic models and/or grid spacing. Global grids have been provided as companion grids in several other studies (e.g. Richards et al., 2018; Straume et al., 2019).

The advent of full-plate reconstructions with continuously evolving plate polygons (Gurnis et al., 2012) has allowed the development of new approaches to the creation of seafloor age grids. These methods use the definition of mid-ocean ridge locations and the plate rotation parameters from the underlying plate model to create and reconstruct parcels of seafloor through their plate tectonic history (Karlsen et al., 2020; Merdith et al., 2019; Williams et al., 2020). These approaches are useful for on-the-fly creation of age grids and for approximating the global age of the ocean crust, especially for times in the past where most of the seafloor being reconstructed has since been subducted and therefore no constraints are available on precise spreading geometries and asymmetries. However, for seafloor preserved at present day where magnetic anomalies are available (in particular where both flanks of a spreading system are preserved), direct interpolation between the isochrons will more accurately reflect spreading history and allows parameters such as spreading rate, asymmetry and obliquity to be extracted.

Recent advances have necessitated an update to the global age distribution of the oceanic crust. These significant advances include: major updates to the global plate motion model that underpins the crustal age model (Seton et al., 2012; Müller et al., 2016a; Müller et al., 2019); a repository for the world's magnetic anomaly identifications (Seton et al., 2014)—one of the primary building-blocks for global plate reconstructions and crustal age determination; and a

digital dataset of the world's transform faults and fracture zones (Matthews et al., 2011; Wessel et al., 2015), which helps constrain present and past plate motions. In this paper, we present an updated model for the present-day age of oceanic crust underpinned by these new advances. The present-day age grid is accompanied by a global age grid misfit grid (with a comparison to previous iterations of the age grid) as well as grids of seafloor-spreading rate, spreading asymmetry, spreading direction and spreading obliquity. All data are made publicly available as either shapefiles or netCDF grids, and can be visualised online through the GPlates portal, http://portal.gplates.org (Müller et al. 2016b). In addition, the workflows to create our age grid and companion grids are publicly available, allowing anyone to reproduce our grids or create their own for alternative reconstructions.

2 Components in building an age model of the oceanic crust

2.1 Magnetic anomaly identifications

Magnetic anomaly identifications underpin plate tectonic reconstructions and form the primary dataset from which the age of the oceanic crust and seafloor-spreading regimes can be determined. The establishment of a repository and standardised format for over 96,000 previously published magnetic anomaly identifications (Seton et al., 2014), which forms part of the Global Seafloor Fabric and Magnetic Lineation (GSFML) repository, has allowed for a more straightforward approach to assess competing plate tectonic interpretations and the consistency between magnetic anomaly identifications and global seafloor-spreading models. The repository also highlights those areas where magnetic anomaly interpretation is hampered either by a paucity of publicly available magnetic data or by the nature of the physical properties of the crust, such as the direction of magnetization of the rocks relative to the direction of the ambient magnetic field (e.g. Equatorial Atlantic), its formation during a period of magnetic reversal quiescence (e.g. the Cretaceous Normal Superchron) or post accretion thermal disturbances (e.g. due to heavy sedimentation (Granot and Dyment, 2019) or intraplate volcanism (e.g. Thoram et al, 2019)).

The GSFML repository presents a collection of publicly available magnetic anomaly identifications and does not discriminate between alternative interpretations. This means that for many areas or spreading corridors, magnetic anomaly identifications from different studies are included that may contradict each other, result in duplicate entries or be superseded by more recent work. While the repository was deliberately designed in this way, there is a need to produce a single global set of magnetic anomaly identifications consistent with a global plate motion model. In updating our present-day age grid model, we create a preferred global set of magnetic anomaly identifications (Fig. 1) consistent with the plate motion model of Müller et al. (2019) and a set of seafloor-spreading isochrons. Synthetic seafloor-spreading isochrons are also created in areas where there is no data, based on the underlying plate tectonic model. The set of magnetic anomaly identifications has been quality-checked and only those that are attributed to a peer-reviewed publication are included.

2.2 Global fracture zone dataset

Fracture zones represent the primary tectonic fabric of the ocean basins and provide crucial constraints on both the direction and speed of relative plate motion. These linear structures trace the direction of seafloor spreading at mid-ocean ridges, and their spacing reflects segmentation at the ridge, which is in turn dependent on spreading rate (e.g. Sandwell & Smith (2009)). Furthermore, their appearance and disappearance in the tectonic fabric of the seafloor

can signify times of spreading center reorganizations (Cande et al., 1988; Matthews et al., 2011), including ridge extinction or relocation events, as well as spreading rate changes.

Matthews et al. (2011) digitized a global fracture zone map based on the gridded satellite-derived vertical gravity gradient (VGG) dataset of Sandwell and Smith (2009). The fracture zones were traced along their VGG minima, the clearest signal to identify in the satellite data. The Matthews et al. (2011) dataset was updated by Wessel et al. (2015) using the improved VGG dataset of Sandwell et al. (2014), which allows structures as small as 6 km in width to be resolved. A key update to the fracture zone dataset is the extension of existing fracture zones and identification of new fracture zones in older crust, closer to continental margins (Wessel et al., 2015). This improvement to the fracture zone data set resulted from a reduced noise level in the VGG data of Sandwell et al. (2014), which better illuminates deeper and more highly sedimented regions compared to previous releases of the VGG grids.

The present-day age grids provide better alignment, compared to previous versions of the age grid, to the latest fracture zone dataset (Wessel et al., 2015). The seafloor-spreading isochrons in the Pacific, Atlantic and parts of the Indian Ocean have been adjusted to be consistent with this dataset. The fracture zones reveal the locations and widths of the present-day and paleo spreading corridors, form a valuable constraint on the shapes of the seafloor isochrons and were directly used for computing finite rotations with uncertainties in selected areas.

2.3 Continent-ocean boundaries (COBs)

In developing a present-day seafloor age grid, it is necessary to define a boundary that distinguishes between regions where the basement rocks underlying the seafloor are considered oceanic in origin (crust formed by seafloor spreading), and regions where the basement rocks are considered to be continental. At active margins this boundary is defined by the interface between downgoing oceanic slabs and the overriding continents. At passive margins formed by continental rifting, the distinction is often more ambiguous. Studies of rifted margins reveal that the process of rifting and final continental breakup can be complex and diverse (Peron-Pinvidic et al., 2013; Reston & Pérez-Gussinyé, 2007), though not always (e.g. Larsen et al. (2018)). In more complex regions, the crust that is clearly oceanic may be separated from continental crust by zones of ambiguous crust, several tens of kilometres wide, whose interpretation is cryptic from geophysical data and sparse geological sampling (e.g. Eagles et al., 2015; Williams et al., 2019). Seafloor underlying these regions has been interpreted to form by a combination of magmatism and exhumation of mantle rocks along detachment faults (e.g. Gillard et al., 2016), similar to the processes operating at slow-spreading ridges in the deep ocean (Reston, 2018; Sauter et al., 2013). In view of these issues, a few points should be kept in mind when using the age grid close to passive margins: (1) the sharp boundary between oceans and continents used for the seafloor age grid is a necessary simplification of more complex continent ocean transition zones. Studies for which the COB location is a critical parameter should take these uncertainties into account (e.g. Brune et al. (2016); Hosseinpour et al. (2013); Williams et al. (2019)), and (2) the monotonic increase in age towards the COB will not account for more complex processes of seafloor generation in areas where seafloor formation was controlled by detachment faulting. For more detailed treatments of different regions that have changed since the Müller et al. (2008) grid, we refer readers to the Supplementary section.

2.4 Seafloor-spreading isochrons and underlying plate model

The seafloor spreading and underlying plate model that underpins the present-day age and accompanying grids is based on Müller et al. (2019) v2.0 (Fig. 1). This model includes several important updates since the Müller et al. (2008) age grid, which are documented in detail in the Supplementary section. The resolution of the datasets presented in this study is dependent on the resolution of our underlying data (i.e. the plate motion model and set of seafloor-spreading isochrons) and is typically every 5–10 million years (see Müller et al., 2016a, for details). It is therefore important to recognise that changes in seafloor-spreading parameters may not necessarily be reflected by a change at our selected stage boundaries. Age and spreading parameter values are also linearly interpolated between stages. The resolution could be improved by decreasing the spacing between rotations in the underlying model but such changes have their own drawbacks as reconstructions based on sets of magnetic anomalies closely spaced in time (i.e. on the million year time scale) are known to increase the noise-to-signal ratio in the data, leading to geodynamically unreasonable behavior (Iaffaldano et al., 2014).

Our model uses the timescale of Gee and Kent (2007), which is largely a combination of Cande and Kent (1995) and Channell et al. (1995). Ages quoted in this paper and the figures (unless otherwise stated) are based on this timescale. We have created a companion set of data and grids consistent with the GTS2012 timescale (Gradstein et al., 2012) for those who may prefer this timescale and also for comparison (Fig. S1).

2.5 Gridding algorithms

The gridding algorithms we use to generate a present-day crustal age and companion grids make use of a Python program called *isopolate*. *Isopolate* generates interpolated seafloor-spreading isochrons based on a set of finite rotations, and files that contain continental-oceanic boundaries, seafloor-spreading isochrons and present-day and extinct ridges. Details about *isopolate* can be found in the Supplementary section. Once the dense set of seafloor spreading isochrons have been generated, we use GMT 6 (Wessel et al., 2019) to generate a median value for each grid cell as a pre-processing step and apply a linear spherical interpolation between isochrons using "sphinterpolate" (Renka, 1997a, 1997b) (Fig. 1). Spreading rate parameter grids use the "surface" function in GMT (Figs. 3-5). The inclusion of spherical interpolation in the gridding workflow has significantly improved the age grid interpolation for the Arctic region, and across the anti-meridian.

2.6 Age grid misfit and measure of confidence

In previously published versions of the age grid, a measure of the age grid error was provided by assessing the fit between our preferred magnetic anomaly identifications dataset and the seafloor-spreading isochrons derived from the underlying plate motion model. Rather an uncertainty or error, this is more akin to a measure of misfit between the input data and the resultant age grid. We improve on this methodology (Fig. 2) by: i) incorporating the location and age of known extinct ridges (using a subset of MacLeod et al. (2017)) as their location can be traced from the seafloor fabric and age inferred from adjacent magnetic anomaly picks; ii) providing a misfit parameter for our continent-ocean boundaries based on the difference between the age grid and the age according to the break-up time from the plate model and iii) testing alternative upper limit of misfit (Fig. S2).

While the misfit grid is an important measure of the internal consistency of our resultant grid with the data, it does not include a measure of other sources of uncertainty that are much more difficult to quantify. These primarily result from uncertainties in the seafloor-spreading histories in the underlying plate tectonic model, which can be much larger than the errors related to data misfit. For example, our incorporation of newly identified magnetic anomalies in the eastern Mediterranean (Granot, 2016) has led to an 80 Myr increase in the age of this basin as compared to previously published models, which far outweighs any error related to misfit. To capture an element of this uncertainty, we created a confidence grid (Fig. 6), which assigns areas of high and low confidence based on our gridded data sets. Lower confidence is assigned when one of the following conditions are met: i) the age uncertainty is greater than 4 times the global mean; ii) the age of the crust falls within the Cretaceous Normal Superchron and in areas of diffuse deformation; iii) spreading symmetry is less than 25% or greater than 75%; iv) spreading obliquities are greater than 45° (indicate fracture zones) and; v) difference between our two alternative timescales is 4 times greater than the mean.

3 Results and discussion

3.1 Age distribution of the world's oceanic crust

Our improvements in constraining the age of the oceanic crust have resulted in an older mean age of 64.2 Myrs compared to previous models (e.g. 63.8 Myrs, Müller et al., 2008, and 61.8 Myrs, Müller et al., 1997) (Fig. S3). The misfit parameter is 0.9 Myrs considering an upper bound of 10 Myr (consistent with Müller et al., 2008 and Müller et al., 1997) and 1.8 Myrs considering an upper bound of 20 Myr (consistent with Wright et al. 2020; Fig. 2). A comparison of misfit parameters from previous models are found in Fig. S5. While a small portion of the difference between age grids can be accounted for by the adjustment to the Mesozoic timescale, the majority of the difference can be explained by regional updates in the seafloor-spreading histories and adjustments to the area of defined oceanic crust. Our improvements to the misfit workflow and updates to the seafloor-spreading model in some key regions has resulted in a reduction in the error by 0.4 Myrs between this model and Müller et al. (2008).

The mean crustal age of the Atlantic Ocean is 69.2 Myrs (Fig. S3–4) and remains, on average, the oldest of the major ocean basins. Most significantly, there is now a more prominent population of early Jurassic-aged ocean floor in the Central and Equatorial Atlantic (west of the Demerara Rise, in the Gulf of Cadiz, and an increase in the area of older ocean floor offshore Central Atlantic) (Fig. S4). The increase in mean age is partly offset by the introduction of two extinct spreading ridges in the South Atlantic during the Cretaceous Normal Superchron (CNS), which replace older crust with slightly younger crust formed during the CNS, and adjustments to the continent-ocean boundaries in the North Atlantic.

The mean crustal age of the Pacific Ocean is 65.7 Myrs (Fig. S3–4). The main changes to the Pacific include an expanded area of Jurassic ocean floor around the Pacific triangle, constrained by new (but sparse) magnetic anomaly identifications (Tivey et al., 2006; Tominaga et al., 2015); improvements in the younger history of the eastern Pacific due to the incorporation of a rotation model for several microplates (e.g. Buenaventura, Malpelo, Mathematician, Rivera, Sandra) (McGirr et al. 2020; Wright et al., 2016) and tighter constraints on the 0–83 Ma rotation history of the Pacific Plate (Wright et al., 2015; Wright et al., 2016).

The Indian Ocean is, on average, the youngest ocean basin at 60.0 Myrs (Fig. S3–4). The main changes include an older age of the Mesozoic east African margin, adjustments to the Mesozoic eastern Indian Ocean, changes to the Wharton Basin based on the updated Australia–Antarctica spreading model of Whittaker et al (2013), minor adjustments to the plate model due to the introduction of the Somali plate related to East Africa break-up, and the introduction of a ridge jump in the spreading corridor between Madagascar and Antarctica.

The marginal and back-arc basins have an average age of 47.8 Myrs and have resulted in the largest change in mean age between models. We have incorporated a large number of Cenozoic marginal and back-arc basins that were missing from previous iterations (see Supplementary section and Fig. S3–4) and updated the model of the eastern Mediterranean based on Granot (2016). While the area of oceanic crust in the eastern Mediterranean is small, the inclusion of this crust in the eastern Mediterranean results in the largest difference in age (~80 Myrs) between this model and previously published versions of the age grid.

3.2 Age grid comparison based on alternative timescale and models

We have created a complementary age grid based on the GTS2012 (Gradstein et al., 2012) timescale, which has become the international standard, even though the Gee and Kent (2017) timescale is preferred by those who look at the marine magnetic anomaly record (e.g. Seton et al., 2009; Torsvik et al., 2009). The GTS2012 grid results in an average age of the oceanic crust of 65.2 Myrs, one million years older than Gee and Kent (2007). The increase in average age is primarily driven by the older age assignment to M0 (125.9 Ma) in GTS2012 compared to 120.6 Ma in Gee and Kent (2007), and smaller differences in an older age assignment from M0 to late Jurassic times (Fig. S1). The only notable time where younger ages are predicted in GTS2012 is between 57.1 and 62.5 Ma (Fig. S1), resulting in an increase in seafloor-spreading rate during this period, most notably along the East Pacific.

An alternative age grid presented in Straume et al. (2019) calibrated to the GTS2012 timescale has a mean age of 64.5 Ma (no error grid provided), which is slightly younger but within the misfit bounds to our equivalent GTS2012 model. While there is a slightly larger area of Jurassic-aged crust in the western Pacific and an absence of some Cenozoic back-arc basins, these older ages are offset by areas of younger ocean floor, which are an artefact in their model, particularly in relation to the extent of non-oceanic crust and linear interpolation between discrete smaller ocean basins. This is particularly acute in the Cenozoic back-arc basin regions of SE Asia, SW Pacific and Caribbean (Fig. S5).

Another alternative age grid model, presented by Richards et al. (2018), modified the present-day age grid released in the Müller et al. (2016a) data bundle to include an updated opening history of the Gulf of California, the incorporation of Mesozoic crust underlying the Black, Caspian and eastern Mediterranean seas and the Cenozoic New Caledonia and Aleutian basins. While updates to the Gulf of California, eastern Mediterranean and Aleutian basins are part of our updated age grid, we do not include the speculative oceanic crust that may underlie the Black and Caspian seas and New Caledonia Basin.

3.3 Seafloor-spreading rate, asymmetry and obliquity

We present grids of spreading rate, asymmetry, direction and obliquity (Figs. 3-5). Spreading rate is computed both as a full spreading rate (values reported in this study), which calculates spreading velocities between two sets of isochrons at the time of crustal accretion, and a half spreading rate, which is calculated relative to the mid-ocean ridge and takes into account

spreading asymmetry. Spreading asymmetry is calculated by determining the percentage of crustal accretion between pairs of adjacent isochrons by dividing the angular distance between them by the full stage rotation angle (Müller et al., 2008). Spreading obliquity is the angle between the spreading direction and ridge normal direction. Spreading direction is useful for comparing to larger scale geological processes, such as seismic anisotropy (e.g. Becker et al., 2014) and absolute plate motion (Williams et al., 2016) but is not a parameter we consider in this study. The details on how these spreading parameters are computed within *isopolate* are described in the Supplementary section.

For the purpose of analysis, we have separated our data into five spreading modes according to Dick et al. (2003): ultra-slow (<20 mm/yr), slow (20–55 mm/yr), intermediate (or transitional between slow and fast) (55–75 mm/yr), fast (75–180 mm/yr) and superfast (>180 mm/yr). The thresholds for each spreading rate mode are primarily based on differences in axial relief and crustal thickness, with ultra-slow systems additionally based on the absence of transform faults and volcanism (Dick et al., 2003). We assess spreading asymmetry and obliquity according to these spreading rate classes.

We find that ocean floor generated at ultra-slow spreading systems (<20 mm/yr), such as the presently active SW Indian Ridge, Gakkel Ridge and North Atlantic, account for only 5% of the global total by area (Fig. 3). Other periods of ultra-slow spreading still preserved at present-day but currently inactive are unsurprisingly mainly associated with the early stages of continental break-up, for example, along the Central Atlantic, Labrador Sea and Baffin Bay, and Australian-Antarctic margins. These ultra-slow spreading systems exhibit higher asymmetry (symmetric spreading only accounting for 48% of the crust generated) compared to slow-intermediate spreading systems (Fig. 4 and S8). Complexities in spreading close to continental margins, immediately following continental break-up may explain part of this asymmetry while another factor may be that seafloor-spreading isochrons are closely spaced in ultra-slow systems so any inaccuracies in their location may amplify an artefact in the data set. A wide distribution of spreading obliquity is also observed. Spreading with minimal obliquity (0–5°) only accounts for 22% of the total, with a gradual linear decrease towards 45°, except for a small increase between 30–35° (Fig. 5). Over 45% of crust forms with greater than 15° of obliquity. Combined, these parameters support the non-traditional nature of seafloor spreading at ultra-slow systems, where there is known to be greater segmentation and areas of mantle exhumation.

Ocean floor generated at slow spreading systems (20–55 mm/yr) accounts for 33% of the global total (or 36% if using GTS2012) and is the second most common type of seafloor spreading in preserved ocean floor based on the criteria adopted in our study. Slower spreading ridges generate less crust, therefore these values indicate a proportionally higher amount of ultra-slow to slow mid-ocean ridges than fast and super-fast ridges, consistent with the study of Dick et al. (2003) who report ultra-slow spreading ridges make up ~36% of the present-day global ridge system. Examples of these spreading systems operating at present day include the majority of the Atlantic spreading ridges, Pacific–Antarctic Ridge and the Carlsberg Ridge (Fig. 3). In the past, slow spreading dominated parts of the Mesozoic East African basins, Weddell Sea and Tasman Sea. Crustal accretion at slow spreading crust is relatively stable with 75% of all crust formed at slow spreading ridges exhibiting only a minor, within 5%, amount of asymmetry and 98% of crust is generated within 25% of symmetry (Fig. 4 and S8). A marked change in the distribution of spreading obliquities occurs between ultra-slow and slow spreading systems from a linear trend towards a more exponential trend. Low degrees of obliquity (0–5^{o}) account for 35% of the total, with decreasing values towards 45^{o} except for a

small increase between 25–30° (Fig. 5). This decrease in obliquity with increasing spreading rate is consistent with the studies of Atwater and Macdonald (1977) and Zhang et al. (2018), while the small uptake in obliquities between 25–30° may reflect the uptake according to Zhang et al. (2018). Only 25% of crust is formed via spreading that has greater than 15° obliquity.

Intermediate spreading systems (55–75 mm/yr), classified as transitional between slow and fast spreading according to Dick et al. (2003), account for 20% of the global total and dominate present-day spreading along the Australian–Antarctic Ridge and much of its established seafloor-spreading history (Fig. 3). In the past, the Mesozoic southern South Atlantic, the western Australian basins, last stages of Kula Plate spreading and pockets of spreading in the SE Pacific Ocean are characterised by intermediate seafloor spreading (Fig. 3). Crustal accretion is quite stable at intermediate spreading regimes, with 69% of crust generated within 5% of symmetry (Fig. S8) and 96% within 25% of symmetric spreading. Spreading is not very oblique, with 54% of crust generated within 0–5° of being directly aligned with the spreading direction (Fig. 5).

We find that fast seafloor-spreading systems (75–180 mm/yr) account for 39% of the global total of oceanic crust (or 37% using GTS2012) and are the most common type of seafloor spreading in preserved ocean floor based on the criteria adopted in our study. The two prominent regions of fast spreading covers much of the Cenozoic and Mesozoic Pacific Ocean and large sections of the Indian Ocean, particularly for the time period before India-Eurasia collision ~45–40 Ma (Fig. 3). Fast spreading rates are absent from the Atlantic Ocean. The degree of asymmetric spreading increases as the spreading rate increases. Only 53% of crust forms within 5% of symmetry and 90% within 25% of symmetry (Fig. 4). Some of the asymmetries reflected at these higher spreading rates may be artificial and rather reflect that these areas are missing a model for more localised, complex seafloor spreading (e.g. microplate formation, ridge jumps). Spreading obliquities exponentially decrease from 0 to 45°. Only 15% of crust forms when spreading obliquity is greater than 15° and 46% of crust forms with little/negligible obliquity (between 0–5°) (Fig. 5). While Zhang et al. (2018) suggest an increase in spreading obliquity at super-fast spreading rates (equivalent to the high-end of our fast rates), we do not see this strongly reflected in our data.

Super-fast spreading (>180 mm/yr) can be found in small pockets in the Pacific Ocean (Fig. 3) and accounts for 3% of the global total. This value is likely to be artificially high as they may reflect an incomplete seafloor-spreading record, for example missing microplate formation or ridge jumps, which are characteristic of higher spreading rates. Spreading asymmetries likely suffer from the same limitations as we can see that only 55% of crust falls with 5% of symmetric spreading (Fig. 4 and S8). Within super-fast systems, there is very little oblique spreading (63% forms within 0–5° obliquity and only 5% of crust forming at obliquities greater than 15°) (Fig. 5).

On the whole, ultra-slow, slow and intermediate systems dominate the Atlantic and Indian oceans and exhibit the most symmetric spreading and highest overall obliquity. This may be a consequence of the shorter length of subduction (and therefore slab pull) along the margins of these ocean basins driving their opening. This is in contrast to the Pacific, which has been surrounded by subduction zones throughout much of its Mesozoic to Cenozoic history and as a consequence exhibits higher spreading rates and asymmetry within its preserved crust (Fig.

3-4). Further work to explore the driving forces behind the different dominant modes of spreading in each ocean basin is warranted.

3.4 Confidence grid and limitations

Our quantification of areas that are well constrained (high confidence) and less well constrained (low confidence) is presented through our confidence grid (Fig. 6). High confidence areas are unlikely to change in future iterations of the age grid. Low confidence areas represent areas that may have a change in age assignment in the future with new data, a new seafloor-spreading model or increased resolution of the data. Low value areas are assigned based on the age misfit, the CNS, spreading asymmetry, spreading obliquity and timescale.

For the misfit parameter in the context of the confidence grid, we base a low confidence classification where the misfit grid has values more than 4 times the mean**.** These areas include: ocean floor that formed during the CNS where no magnetic anomaly constraints exist; the equatorial Atlantic where no magnetic anomaly signatures can be identified because of the orientation of spreading relative to the latitudinal position of the crust at the time of formation; the Pacific triangle due to a paucity of robust magnetic anomaly identifications, especially those that extend beyond 160 Ma; areas close to the continental margins where the complexities of continental extension and break-up are not accounted for in the underlying plate motion model; and areas where extinct spreading centres have yet to be identified or incorporated into the underlying model (Fig. 2).

Low confidence is also assigned if crust falls within the Cretaceous Normal Superchron (CNS). While we know that crust that formed during the CNS must have formed at least between ~83 Ma and ~120–125 Ma (depending on the timescale used), we have few constraints on what happened within this time range. These areas could be improved in future versions of the age grid by incorporating ages from magnetic anomalies due to variations in the strength of the dipolar geomagnetic field (Granot & Dyment, 2015; Granot et al., 2012) and will be a focus for further work.

Low confidence values are also accompanied with anomalously high or low spreading asymmetry values. As previously touched on, the temporal resolution of our dataset is controlled by the resolution of the underlying plate model (~5–10 Myrs). This means that changes occurring between these time periods (i.e. smaller scale complex spreading systems or plate motion changes) may be missed, with implications for the robustness of the crustal age and seafloor-spreading parameters (primarily the rate and asymmetry) in some areas. For example, fast spreading systems appear to have extremely high crustal asymmetries in some areas (Fig. 4), but the high asymmetries can at least be partly attributable to missing microplate formation and spreading complexities. The East Pacific Rise is an example of a fast spreading system where we have incorporated some extinct microplates, such as the Bauer and Mathematician microplates, but have yet to incorporate the active Easter and Juan Fernandez microplates and the extinct Friday, Hudson, and Selkirk microplates (see Matthews et al., 2016). In the Indian Ocean, the area of major asymmetric spreading west of the Ninetyeast Ridge (Fig. 4) corresponds to crust that formed during the rapid northward motion of the Indian plate. This crust also includes the Mammerickx Microplate, which formed around 47 Ma (Matthews et al., 2016), related to the time of the India–Eurasia collision (Cande & Patriat, 2015). This microplate has not been incorporated in our age grid. It is likely that there are other

undocumented microplates in the Indian Ocean, particularly during the time of fast spreading rates and where anomalously high spreading asymmetries have been mapped, and our datasets could be used as a basis for targeted data collection and interpretation in these areas (Fig. 4).

Spreading obliquities greater than 45° are also assigned as low confidence areas as these likely indicate crust that was formed within fracture zone segments and therefore prone to high uncertainties. Low confidence is also assigned to those areas where there has been a large (greater than 4 times the mean) change in the age based on timescale alone.

An important consideration when assessing our confidence grid is that we assume that our preferred picks and plate reconstructions are the right ones. Our confidence grid does not take into account that alternative interpretations exist for some areas, areas of diffuse deformation (e.g. DeMets et al., 2005), or that, regardless of whether or not competing interpretations exist for certain spreading sequences, the magnetic anomaly identifications could potentially be erroneous. While lower confidence does not mean that our data sets are wrong in those areas, they provide an important companion data set to our age and spreading parameter grids particularly for non-experts who may not appreciate the inherent uncertainties in age and plate models.

The confidence grid additionally allows us to highlight those areas of the ocean floor that are either in need of re-interpretation to clarify the interpretation of the magnetic anomaly identifications or areas that are lacking publicly available magnetic anomaly pick interpretations or data (Fig. 6). These areas include crust formed during the CNS, the Mesozoic Pacific triangle, section of the East Pacific Rise and fast-spreading crust in the Indian Ocean. The collection of additional magnetic anomaly data and/or the reinterpretation of existing data should be prioritised for these areas.

4 Conclusions

We present an updated oceanic crustal age grid together with grids for complementary seafloor-spreading parameters including rate, asymmetry and obliquity. We find that the mean age of oceanic crust is 64.2 Myrs, slightly older than previous estimates and 1 Myr older if using the GTS2012 timescale. The distribution of spreading modes in the preserved seafloor-spreading record is relatively equal between slow (33%) and fast (39%) systems. Slow and intermediate spreading systems exhibit the most stable behavior in terms of spreading asymmetry and obliquity and ultraslow systems exhibit highly asymmetric and more oblique spreading, consistent with previous studies. Understanding these parameters in the preserved seafloor-spreading record can provide a framework to better inform reconstructions of synthetic ocean floor by providing a range of possible values that are typical of oceanic spreading and constraints on the limits of more extreme behavior. We provide a confidence grid to provide guidance to scientists using our datasets to pin-point areas where our model and grids are poorly constrained thus indicating where additional effort and resources should be invested in further data collection and interpretation.

Acknowledgments, Samples, and Data

We would like to acknowledge funding from the Australian Research Council through grants FT130101564 (MS), DP200100966 (MS and SEW), IH130200012 (RDM and SZ),

DP180102280 (JW and SEW), Alfred P Sloan grants G-2017-9997 and G-2018-11296 (SZ, RDM and SW), and a University of Sydney Robinson Fellowship (SZ).

All gridded datasets and datafiles associated with this paper as well as the workflows can be downloaded from https://earthbyte.org/webdav/ftp/earthbyte/agegrid/2020/. The global plate motion model can be found at https://www.earthbyte.org/webdav/ftp/Data_Collections/Muller_etal_2019_Tectonics.

References

Atwater, T., & MACDONALD, K. C. (1977). Are spreading centers perpendicular to their transform faults? *Nature, 270*(5639), 715-719.

Becker, T. W., Conrad, C. P., Schaeffer, A. J., & Lebedev, S. (2014). Origin of azimuthal seismic anisotropy in oceanic plates and mantle. *Earth and Planetary Science Letters, 401*, 236-250.

Brune, S., Williams, S. E., Butterworth, N. P., & Müller, R. D. (2016). Abrupt plate accelerations shape rifted continental margins. *Nature, 536*(7615), 201-204.

Cande, S. C., & Kent, D. V. (1995). Revised calibration of the geomagnetic polarity timescale for the Late Cretaceous and Cenozoic. *Journal of Geophysical Research: Solid Earth, 100*(B4), 6093-6095.

Cande, S. C., LaBrecque, J. L., & Haxby, W. F. (1988). Plate kinematics of the South Atlantic: Chron C34 to present. *Journal of Geophysical Research, 93*(B11), 13479-13413,13492.

Cande, S. C., & Patriat, P. (2015). The anticorrelated velocities of Africa and India in the Late Cretaceous and early Cenozoic. *Geophysical Journal International, 200*(1), 227-243.

Channell, J., Cecca, F., & Erba, E. (1995). Correlations of Hauterivian and Barremian (Early Cretaceous) stage boundaries to polarity chrons. *Earth and Planetary Science Letters, 134*(1-2), 125-140.

Coltice, N., Seton, M., Rolf, T., Müller, R., & Tackley, P. J. (2013). Convergence of tectonic reconstructions and mantle convection models for significant fluctuations in seafloor spreading. *Earth and Planetary Science Letters, 383*, 92-100.

Crosby, A., & McKenzie, D. (2009). An analysis of young ocean depth, gravity and global residual topography. *Geophysical Journal International, 178*(3), 1198-1219.

DeMets, C., Gordon, R. G., & Royer, J.-Y. (2005). Motion between the Indian, Capricorn and Somalian plates since 20 Ma: Implications for the timing and magnitude of distributed lithospheric deformation in the equatorial Indian Ocean. *Geophysical Journal International, 161*(2), 445-468.

Dick, H. J., Lin, J., & Schouten, H. (2003). An ultraslow-spreading class of ocean ridge. *Nature, 426*(6965), 405-412.

Dutkiewicz, A., Müller, R., Wang, X., O'callaghan, S., Cannon, J., & Wright, N. (2017). Predicting sediment thickness on vanished ocean crust since 200 Ma. *Geochemistry, Geophysics, Geosystems, 18*(12), 4586-4603.

Eagles, G., Pérez-Díaz, L., & Scarselli, N. (2015). Getting over continent ocean boundaries. *Earth-Science Reviews, 151*, 244-265.

Gaina, C., Nasuti, A., Kimbell, G. S., & Blischke, A. (2017). Break-up and seafloor spreading domains in the NE Atlantic. *Geological Society, London, Special Publications, 447*(1), 393-417.

Gaina, C., Van Hinsbergen, D. J., & Spakman, W. (2015). Tectonic interactions between India and Arabia since the Jurassic reconstructed from marine geophysics, ophiolite geology, and seismic tomography. *Tectonics, 34*(5), 875-906.
Gee, J. S., & Kent, D. V. (2007). Source of oceanic magnetic anomalies and the geomagnetic polarity time scale.
Gillard, M., Autin, J., & Manatschal, G. (2016). Fault systems at hyper-extended rifted margins and embryonic oceanic crust: Structural style, evolution and relation to magma. *Marine and Petroleum Geology, 76*, 51-67.
Gradstein, F. M., Ogg, J. G., Schmitz, M., & Ogg, G. (2012). *The geologic time scale 2012*: elsevier.
Granot, R. (2016). Palaeozoic oceanic crust preserved beneath the eastern Mediterranean. *Nature Geoscience, 9*(9), 701-705.
Granot, R., & Dyment, J. (2019). The influence of post-accretion sedimentation on marine magnetic anomalies. *Geophysical Research Letters, 46*(9), 4645-4652.
Granot, R., & Dyment, J. (2015). The Cretaceous opening of the South Atlantic Ocean. *Earth and Planetary Science Letters, 414*, 156-163.
Granot, R., Dyment, J., & Gallet, Y. (2012). Geomagnetic field variability during the Cretaceous Normal Superchron. *Nature Geoscience, 5*(3), 220-223.
Gurnis, M., Turner, M., Zahirovic, S., DiCaprio, L., Spasojevic, S., Müller, R. D., et al. (2012). Plate tectonic reconstructions with continuously closing plates. *Computers & Geosciences, 38*(1), 35-42.
Hosseinpour, M., Müller, R., Williams, S., & Whittaker, J. (2013). Full-fit reconstruction of the Labrador Sea and Baffin Bay. *Solid Earth Discussions, 5*(2).
Iaffaldano, G., Hawkins, R., Bodin, T., & Sambridge, M. (2014). REDBACK: Open-source software for efficient noise-reduction in plate kinematic reconstructions. *Geochemistry, Geophysics, Geosystems, 15*(4), 1663-1670.
Karlsen, K. S., Domeier, M., Gaina, C., & Conrad, C. P. (2020). A tracer-based algorithm for automatic generation of seafloor age grids from plate tectonic reconstructions. *Computers & Geosciences*, 104508.
Larsen, H. C., Mohn, G., Nirrengarten, M., Sun, Z., Stock, J., Jian, Z., et al. (2018). Rapid transition from continental breakup to igneous oceanic crust in the South China Sea. *Nature Geoscience, 11*(10), 782-789.
MacLeod, S. J., Williams, S. E., Matthews, K. J., Müller, R. D., & Qin, X. (2017). A global review and digital database of large-scale extinct spreading centers. *Geosphere, 13*(3), 911-949.
Matthews, K. J., Müller, R. D., & Sandwell, D. T. (2016). Oceanic microplate formation records the onset of India–Eurasia collision. *Earth and Planetary Science Letters, 433*, 204-214.
Matthews, K. J., Müller, R. D., Wessel, P., & Whittaker, J. M. (2011). The tectonic fabric of the ocean basins. *Journal of Geophysical Research: Solid Earth, 116*(B12).
McGirr, R., Seton, M., and Williams, S., 2020, Kinematic and geodynamic evolution of the Isthmus of Panama region: Implications for Central American Seaway closure. *GSA Bulletin* doi: https://doi.org/10.1130/B35595.1
Merdith, A. S., Atkins, S. E., & Tetley, M. G. (2019). Tectonic Controls on Carbon and Serpentinite Storage in Subducted Upper Oceanic Lithosphere for the Past 320 Ma. *Frontiers in Earth Science, 7*(332). Original Research. https://www.frontiersin.org/article/10.3389/feart.2019.00332
Müller, R., Dutkiewicz, A., Seton, M., & Gaina, C. (2013). Seawater chemistry driven by supercontinent assembly, breakup, and dispersal. *Geology, 41*(8), 907-910.

Müller, R. D., Qin, X., Sandwell, D. T., Dutkiewicz, A., Williams, S. E., Flament, N., et al. (2016). The GPlates portal: cloud-based interactive 3D visualization of global geophysical and geological data in a web browser. *PloS one, 11*(3).

Müller, R. D., Roest, W. R., Royer, J. Y., Gahagan, L. M., & Sclater, J. G. (1997). Digital isochrons of the world's ocean floor. *Journal of Geophysical Research: Solid Earth, 102*(B2), 3211-3214.

Müller, R. D., Sdrolias, M., Gaina, C., & Roest, W. R. (2008). Age, spreading rates, and spreading asymmetry of the world's ocean crust. *Geochemistry, Geophysics, Geosystems, 9*(4).

Müller, R. D., Seton, M., Zahirovic, S., Williams, S. E., Matthews, K. J., Wright, N. M., et al. (2016). Ocean basin evolution and global-scale plate reorganization events since Pangea breakup. *Annual Review of Earth and Planetary Sciences, 44*, 107-138.

Müller, R. D., Zahirovic, S., Williams, S. E., Cannon, J., Seton, M., Bower, D. J., et al. (2019). A global plate model including lithospheric deformation along major rifts and orogens since the Triassic. *Tectonics, 38*(6), 1884-1907.

Olson, P., Reynolds, E., Hinnov, L., & Goswami, A. (2016). Variation of ocean sediment thickness with crustal age. *Geochemistry, Geophysics, Geosystems, 17*(4), 1349-1369.

Pérez-Díaz, L., & Eagles, G. (2017). A new high-resolution seafloor age grid for the S outh A tlantic. *Geochemistry, Geophysics, Geosystems, 18*(1), 457-470.

Peron-Pinvidic, G., Manatschal, G., & Osmundsen, P. T. (2013). Structural comparison of archetypal Atlantic rifted margins: A review of observations and concepts. *Marine and Petroleum Geology, 43*, 21-47.

Renka, R. J. (1997a). Algorithm 772: STRIPACK: Delaunay triangulation and Voronoi diagram on the surface of a sphere. *ACM Transactions on Mathematical Software (TOMS), 23*(3), 416-434.

Renka, R. J. (1997b). Algorithm 773: SSRFPACK: interpolation of scattered data on the surface of a sphere with a surface under tension. *ACM Transactions on Mathematical Software (TOMS), 23*(3), 435-442.

Reston, T. (2018). Flipping detachments: The kinematics of ultraslow spreading ridges. *Earth and Planetary Science Letters, 503*, 144-157.

Reston, T. J., & Pérez-Gussinyé, M. (2007). Lithospheric extension from rifting to continental breakup at magma-poor margins: rheology, serpentinisation and symmetry. *International Journal of Earth Sciences, 96*(6), 1033-1046.

Richards, F., Hoggard, M., Cowton, L., & White, N. (2018). Reassessing the thermal structure of oceanic lithosphere with revised global inventories of basement depths and heat flow measurements. *Journal of Geophysical Research: Solid Earth, 123*(10), 9136-9161.

Sandwell, D. T., Müller, R. D., Smith, W. H., Garcia, E., & Francis, R. (2014). New global marine gravity model from CryoSat-2 and Jason-1 reveals buried tectonic structure. *Science, 346*(6205), 65-67.

Sandwell, D. T., & Smith, W. H. (2009). Global marine gravity from retracked Geosat and ERS-1 altimetry: Ridge segmentation versus spreading rate. *Journal of Geophysical Research: Solid Earth, 114*(B1).

Sauter, D., Cannat, M., Rouméjon, S., Andreani, M., Birot, D., Bronner, A., et al. (2013). Continuous exhumation of mantle-derived rocks at the Southwest Indian Ridge for 11 million years. *Nature Geoscience, 6*(4), 314-320.

Seton, M., Gaina, C., Müller, R., & Heine, C. (2009). Mid-Cretaceous seafloor spreading pulse: Fact or fiction? *Geology, 37*(8), 687-690.

Seton, M., Müller, R., Zahirovic, S., Gaina, C., Torsvik, T., Shephard, G., et al. (2012). Global continental and ocean basin reconstructions since 200 Ma. *Earth-Science Reviews, 113*(3-4), 212-270.
Seton, M., Whittaker, J. M., Wessel, P., Müller, R. D., DeMets, C., Merkouriev, S., et al. (2014). Community infrastructure and repository for marine magnetic identifications. *Geochemistry, Geophysics, Geosystems, 15*(4), 1629-1641.
Stadler, G., Gurnis, M., Burstedde, C., Wilcox, L. C., Alisic, L., & Ghattas, O. (2010). The dynamics of plate tectonics and mantle flow: From local to global scales. *Science, 329*(5995), 1033-1038.
Steinberger, B. (2016). Topography caused by mantle density variations: observation-based estimates and models derived from tomography and lithosphere thickness. *Geophysical Supplements to the Monthly Notices of the Royal Astronomical Society, 205*(1), 604-621.
Straume, E., Gaina, C., Medvedev, S., Hochmuth, K., Gohl, K., Whittaker, J. M., et al. (2019). GlobSed: Updated total sediment thickness in the world's oceans. *Geochemistry, Geophysics, Geosystems, 20*(4), 1756-1772.
Thoram, S., Sager, W. W., & Jokat, W. (2019). Implications of Updated Magnetic Anomalies for the Late Cretaceous Tectonic Evolution of Walvis Ridge. *Geophysical Research Letters, 46*(16), 9474-9482.
Tivey, M. A., Sager, W. W., Lee, S.-M., & Tominaga, M. (2006). Origin of the Pacific Jurassic quiet zone. *Geology, 34*(9), 789-792.
Tominaga, M., Tivey, M. A., & Sager, W. W. (2015). Nature of the Jurassic magnetic quiet zone. *Geophysical Research Letters, 42*(20), 8367-8372.
Torsvik, T. H., Rousse, S., Labails, C., & Smethurst, M. A. (2009). A new scheme for the opening of the South Atlantic Ocean and the dissection of an Aptian salt basin. *Geophysical Journal International, 177*(3), 1315-1333.
Van Avendonk, H. J., Davis, J. K., Harding, J. L., & Lawver, L. A. (2017). Decrease in oceanic crustal thickness since the breakup of Pangaea. *Nature Geoscience, 10*(1), 58-61.
Wessel, P., Luis, J., Uieda, L., Scharroo, R., Wobbe, F., Smith, W., & Tian, D. (2019). The generic mapping tools version 6. *Geochemistry, Geophysics, Geosystems*.
Wessel, P., Matthews, K. J., Müller, R. D., Mazzoni, A., Whittaker, J. M., Myhill, R., & Chandler, M. T. (2015). Semiautomatic fracture zone tracking. *Geochemistry, Geophysics, Geosystems, 16*(7), 2462-2472.
Whittaker, J. M., Williams, S. E., & Müller, R. D. (2013). Revised tectonic evolution of the Eastern Indian Ocean. *Geochemistry, Geophysics, Geosystems, 14*(6), 1891-1909.
Williams, S. E., Flament, N., & Müller, R. D. (2016). Alignment between seafloor spreading directions and absolute plate motions through time. *Geophysical Research Letters, 43*(4), 1472-1480.
Williams, S. E., Whittaker, J. M., Halpin, J. A., & Müller, R. D. (2019). Australian-Antarctic breakup and seafloor spreading: Balancing geological and geophysical constraints. *Earth-Science Reviews, 188*, 41-58.
Williams, S., Wright, N. M., Cannon, J., Flament, N., & Müller, R. D. (2020). Reconstructing seafloor age distributions in lost ocean basins. *Geoscience Frontiers,* https://doi.org/10.1016/j.gsf.2020.06.004
Wright, N. M., Müller, R. D., Seton, M., & Williams, S. E. (2015). Revision of Paleogene plate motions in the Pacific and implications for the Hawaiian-Emperor bend. *Geology, 43*(5), 455-458.

Wright, N. M., Seton, M., Williams, S. E., & Mueller, R. D. (2016). The Late Cretaceous to recent tectonic history of the Pacific Ocean basin. *Earth-Science Reviews, 154*, 138-173.

Wright, N. M., Seton, M., Williams, S. E., Whittaker, J. M., & Müller, R. D. (2020). Sea level fluctuations driven by changes in global ocean basin volume following supercontinent break-up. *Earth-Science Reviews*, 103293.

Zhang, T., Gordon, R. G., & Wang, C. (2018). Oblique seafloor spreading across intermediate and superfast spreading centers. *Earth and Planetary Science Letters, 495*, 146-156.

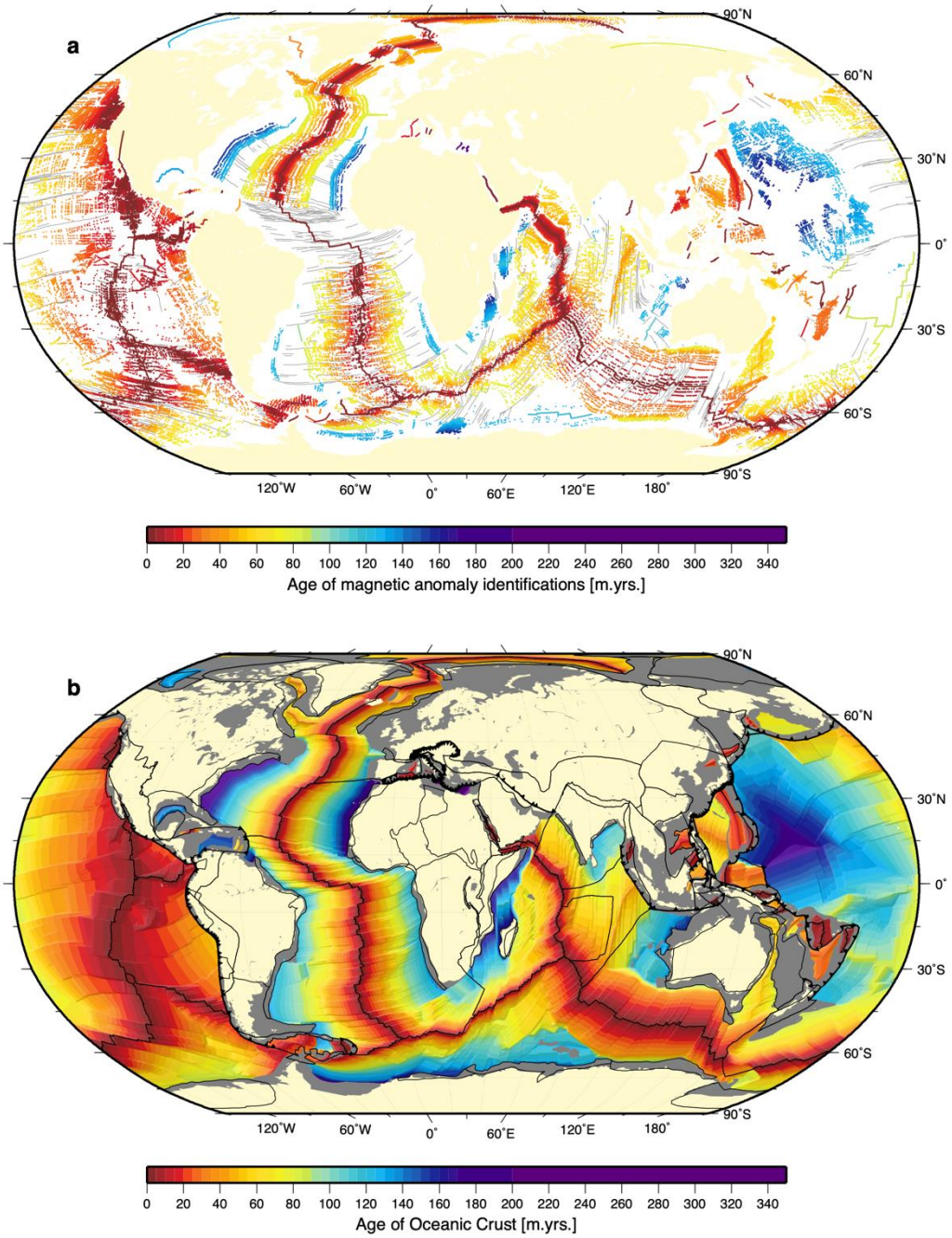

Figure 1. a. Constraints used to derive the present-day map of the age of the oceanic crust. These include a preferred magnetic pick compilation (color coded by age) extracted from magnetic anomaly identifications found on the GSFML website (Seton et al., 2014), active and extinct spreading ridges used in the computation of the age grid and a global map of fracture zones and other tectonic fabric (thin grey lines, (Matthews et al., 2011; Wessel et al., 2015)). Robinson projection centered on 30°E. **b.** Resultant present-day grid of the age of the oceanic crust. Present-day plate boundaries are from the global deforming plate model of Müller et al. (2019) with regions of present-day deformation marked as grey polygons.

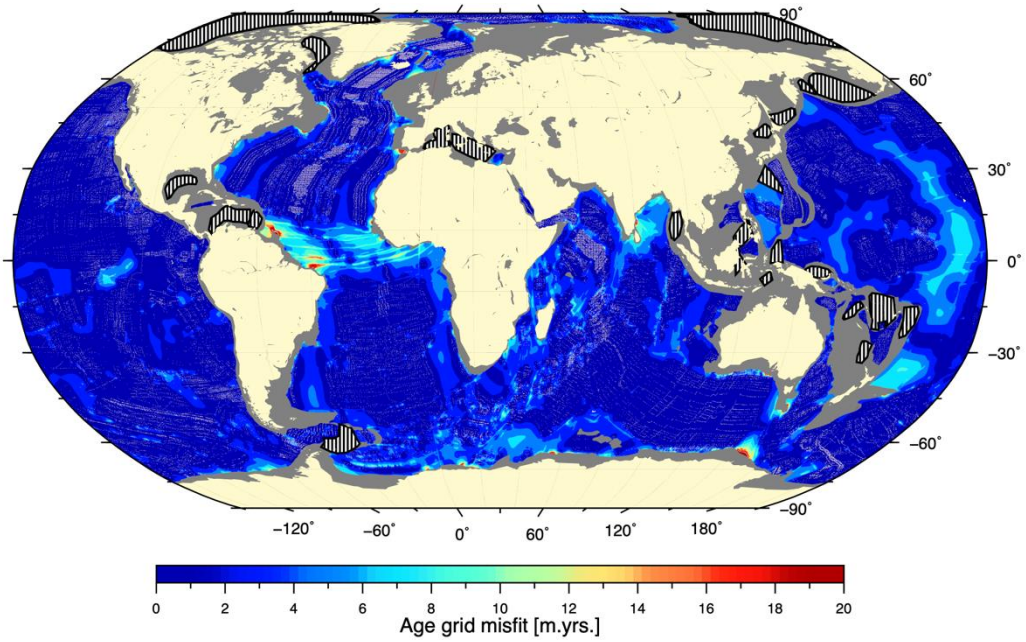

Figure 2: Global grid showing the misfit between the age of the oceanic crust and the age constraints. Magnetic anomaly identifications used in the analysis, including reconstructed identifications, plotted as small white circles. Hatched areas represent enclosed ocean basins (e.g. Caribbean Basin, Gulf of Mexico, Bering Sea) and some back-arc basins that have no magnetic pick constraints.

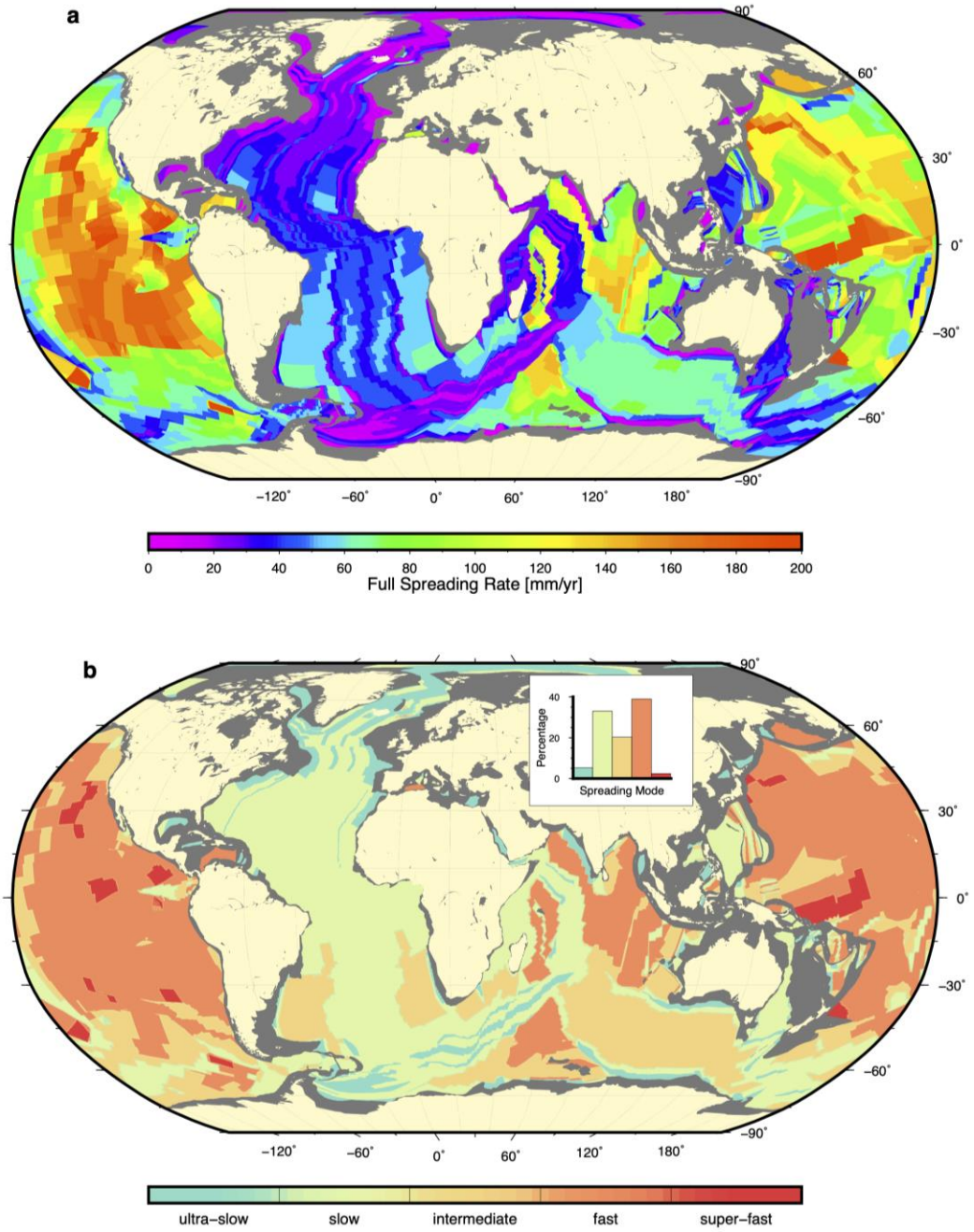

Figure 3a. Present-day seafloor-spreading rate grid **b.** Present-day spreading mode grid. Ultra-slow = < 20 mm/yr, slow = 20–55 mm/yr, intermediate = 55–75 mm/yr, fast = 75–180 mm/yr and superfast = > 180 mm/yr. Histogram insert shows the percentage of each spreading mode.

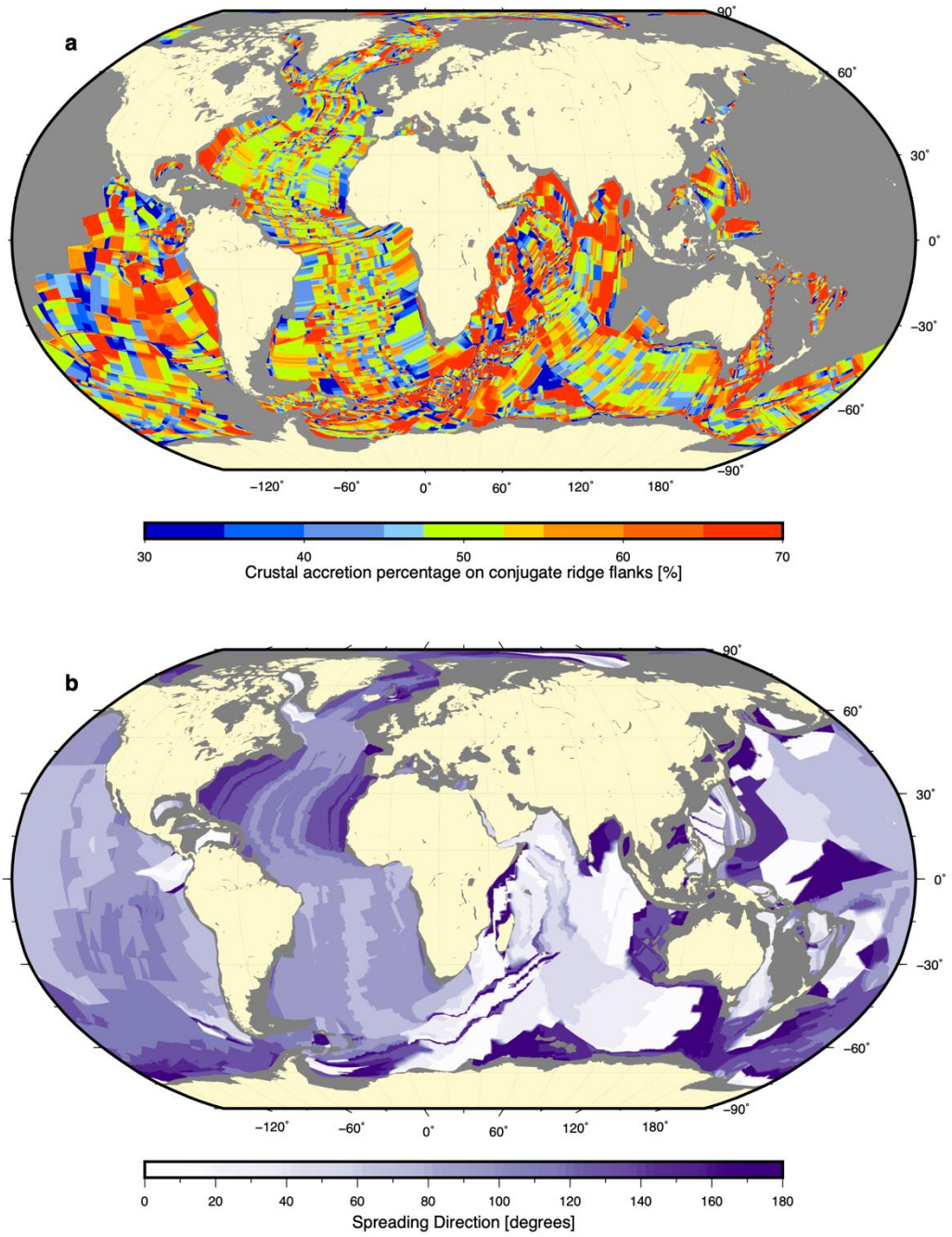

Figure 4a. Present-day asymmetry grid with values of 50% representing symmetric spreading. Areas that do not have a present-day spreading conjugate are masked as grey areas. **b.** Present-day spreading direction grid.

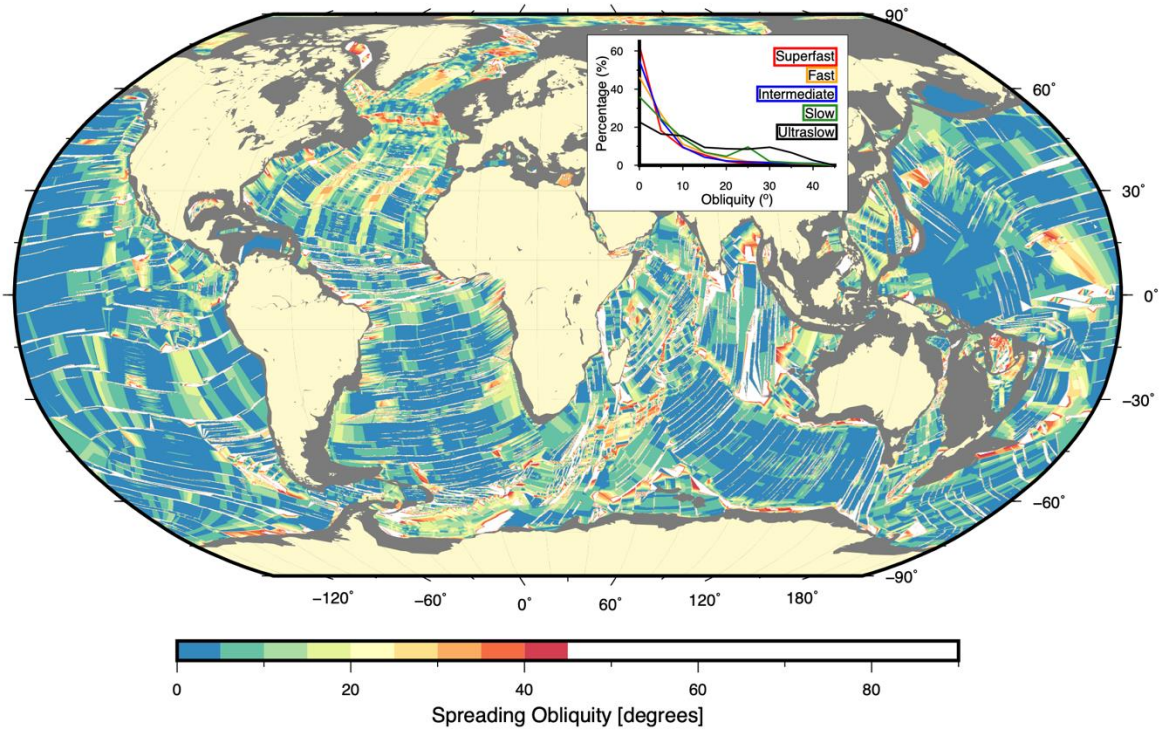

Figure 5. Present-day spreading obliquity grid. Values above 45° indicate fracture zone segments, denoted in white. Insert shows percentage distribution of spreading obliquity separated by spreading mode.

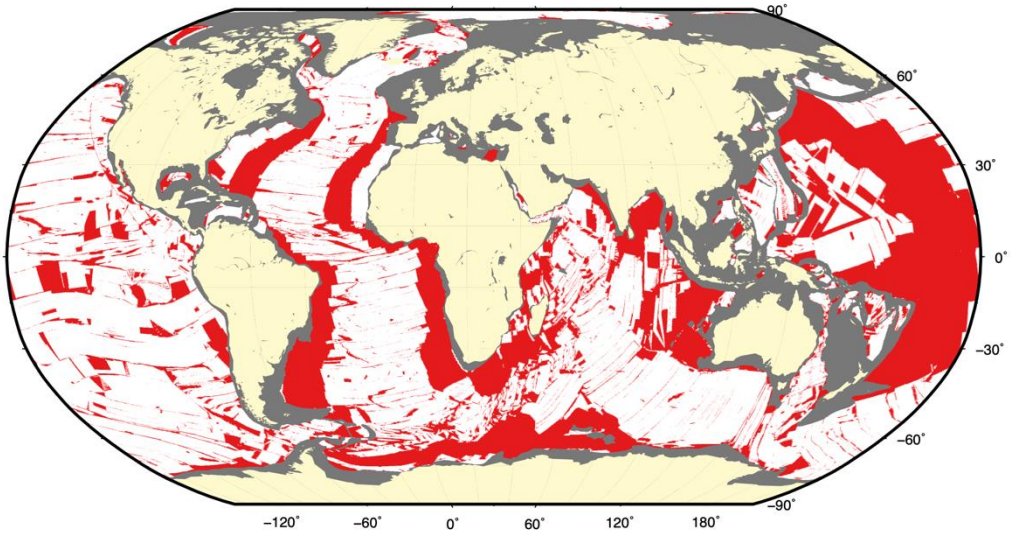

Figure 6: Confidence rating for the present-day age grid highlighting those areas that are poorly constrained (low confidence) based on age, age error, asymmetry, obliquity and timescale (see text for details).